

***Ab initio* investigation of electron capture by Cl^{7+} ions from H**L. B. Zhao,¹ A. Watanabe,² P. C. Stancil,¹ and M. Kimura³¹*Department of Physics and Astronomy and Center for Simulational Physics, University of Georgia, Athens, Georgia 30602-2451, USA*²*Information, Media and Education Square, Ochanomizu University, Tokyo 112-8610, Japan*³*Graduate School of Sciences, Kyushu University, Fukuoka 812-8581, Japan*

(Received 23 March 2007; published 1 August 2007)

An investigation of charge transfer in collisions of ground-state Cl^{7+} with H has been conducted based on a fully quantum-mechanical molecular-orbital close-coupling (QMOCC) approach. The charge-transfer process $\text{Cl}^{7+}(^1S) + \text{H} \rightarrow \text{Cl}^{6+}(2p^6n\ell \ ^2S, ^2P^o, ^2D, ^2F^o, ^2G) + \text{H}^+$ with $n=5$ and 6 is taken into account for collision energies between 10^{-4} eV/u and 1 keV/u. The relevant adiabatic potentials and nonadiabatic coupling matrix elements for the ClH^{7+} system are evaluated with the configuration-interaction method. The investigation shows that electron capture into the $5d$, $5f$, $5g$, and $6p$ states dominates for collision energies less than ~ 1 eV/u, while above 100 eV/u the $5s$, $5p$, $5d$, and $6p$ are the primary capture channels. Comparison with experimental data for collisions of $\text{Cl}^{7+}(^1S)$ with D reveals a discrepancy over the full range of measured energies (5–430 eV/u), while no significant isotope effect is found for QMOCC calculations with deuterium. Furthermore, comparison with a previous calculation of the one-electron $\text{N}^{7+} + \text{H}$ system, as well as measurements of the multielectron $\text{Al}^{7+} + \text{H}$ and $\text{Fe}^{7+} + \text{H}$ systems, suggests that the electronic structure of the core has a non-negligible effect on the charge-transfer process. A one-electron model for relative ℓ distributions is found to agree with the QMOCC results for $n=5$ between 100 and 1000 eV/u, but fails at lower collision energies. Finally, state-selective and total rate coefficients are given for temperatures between 10 and 200 000 K.

DOI: 10.1103/PhysRevA.76.022701

PACS number(s): 34.20.Mq, 34.50.-s, 34.70.+e

I. INTRODUCTION

Charge transfer, or electron capture, in ion-atom and ion-molecule collisions has attracted researchers' attentions for decades because of its application importance in laboratory and astrophysical plasmas [1,2]. Depending on physical conditions, such as temperature and density, charge-transfer reactions may play a crucial role in establishing the ionization balance of the plasmas and may significantly contribute to ion emission spectra by populating excited states of ions. Recent theoretical analyses of x-ray and extreme ultraviolet emission spectra from some comets have confirmed that charge transfer is a major excitation mechanism and is responsible for the major portion of the observed emission [3]. Since many astronomical bodies, such as comets, planetary nebulae, supernova remnants, and the Sun, are too far away to be probed directly, line emission from astronomical objects is frequently used as a diagnostic of their composition and physical properties (see, e.g., [4–6]).

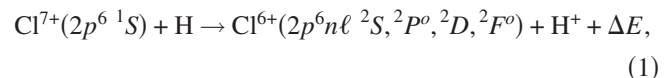
In addition to its importance in the practical applications mentioned above, understanding the dynamics of ion-atom and ion-molecule collisions is also one of the major driving forces for investigations of charge transfer. Such studies provide useful information on molecular structure and interactions in ion-atom and ion-molecule systems. This can be accomplished through comparison of measured and calculated charge-transfer cross sections. The comparisons are also useful to check the validity of classical, semiclassical, and quantal theories describing the collision problems [7] and their valid ranges.

To date, significant progress has been made in laboratory studies of charge transfer (see, e.g., [3]). A great deal of experimental work has been conducted, including measurements of total and state-selective cross sections for exchange of one or more electrons, and detailed, n - and ℓ -resolved line emission spectra for a variety of ion-atom and ion-molecule

systems. Many theoretical approaches, such as quantal and semiclassical molecular-orbital close-coupling [8,9], atomic-orbital close-coupling [10], classical-trajectory Monte Carlo [11], and continuum distorted-wave methods [12], have been developed to describe charge-transfer processes. Applications of these theoretical approaches to individual collisional systems have been reviewed in Ref. [3].

Although electron capture by many ions from atoms or molecules has been reported, both experimental and theoretical data for capture by *heavy* multicharged ions with multi-electron cores are relatively scarce. Experimentally, this is partly due to the difficulty in making sufficiently intense beams at low collision energies [13]. Recently, absolute total integral cross sections for electron capture in collisions of Cl^{7+} with atomic deuterium were measured at the Oak Ridge National Laboratory ion-atom merged-beams apparatus, but no *ab initio* study was performed for the system [13]. Only a fully quantal molecular-orbital close-coupling hidden-crossing calculation was performed for the same charged $\text{N}^{7+} + \text{D}$ system for comparison. The comparison was satisfactory over the energy range 4.6–140 eV/u. Even so, the experiment showed contradiction to the prediction from a simple multichannel Landau-Zener model for Cl^{7+}/D and to measurements for other multicharged ($7+$) ions with multi-electron cores: Fe^{7+} [14] and Al^{7+} [15].

In the present paper, we perform an explicit *ab initio* investigation of electron capture by Cl^{7+} from H by utilizing a fully quantal molecular-orbital close-coupling (QMOCC) approach. The concerned charge-transfer reactions are



with $n=3, 4, 5, 6$, and 7. In Sec. II, calculations of the molecular potentials and nonadiabatic radial and rotational cou-

pling matrix elements for the ClH^{7+} system are described, while Sec. III briefly surveys the QMOCC scattering theory. In Sec. IV, state-to-state, state-selective n - and ℓ -resolved, and total cross sections and rate coefficients are presented and compared to available measurements and calculations. Section V summarizes the main results. Atomic units are used unless otherwise specified.

II. MOLECULAR STRUCTURE CALCULATIONS

The adiabatic potential energy curves and nonadiabatic radial and rotational coupling matrix elements essential to the current collision calculations are obtained with the configuration-interaction method using the quantum chemistry package *ALCHEMY*. Details about the *ALCHEMY* package can be found in Refs. [16,17]. Here we only outline its application to the current problem. The frozen-core approximation is adopted in the calculation. The ten electrons in the 3σ and 1π orbitals are frozen, while one electron in the 36σ , 25π , and 16δ orbitals is treated as active. Slater-type orbitals (STOs) are employed for the atomic basis set. For the chlorine atom, all orbitals up to the $n=5$ manifold are included, while a restricted set of orbitals is considered for $n=6-8$. All orbitals up to $n=2$ are considered for the hydrogen atom [18].

The adiabatic potentials for all molecular electronic states corresponding to the asymptotic limits $\text{Cl}^{6+}(2p^6n\ell)+\text{H}^+$, with $n=3, 4, 5, 6$, and 7 and $\ell=s, p, d, f$, and g , and $\text{Cl}^{7+}(2p^6)+\text{H}$, and nonadiabatic radial and rotational coupling matrix elements between these states were calculated from internuclear distance $R=0.5-29$ a.u. The calculated asymptotic energies are presented for the $20\ ^2\Sigma^+$ and $10\ ^2\Pi$ molecular states relative to the $\text{Cl}^{7+}(2p^6\ ^1S)+\text{H}$ channel and compared with experimental asymptotic atomic energies [19] in Table I. The maximum relative error of the current results from the experimental data is less than 1.94%; less than 0.92% for the dominant capture channels. Because the entrance channel $\text{Cl}^{7+}(2p^6\ ^1S)+\text{H}$ forms only one $^2\Sigma$ state, the $^2\Delta$ states corresponding to $\text{Cl}^{6+}(2p^6n\ell)+\text{H}$ contribute to the charge-transfer reactions (1) only by a two-step rotational coupling interaction, first coupled with $^2\Pi$ and then with $^2\Sigma$. Thus their contribution is expected to be small and they are therefore neglected.

In Fig. 1, the adiabatic potential energies (solid curves) are plotted as a function of internuclear distance R for the 13 molecular states considered in the scattering calculations. The eight $^2\Sigma^+$ and five $^2\Pi$ potentials curves are given in (a) and (b), respectively. Thus only transitions from the $15\ ^2\Sigma^+$ state to $8\ ^2\Sigma^+$, $9\ ^2\Sigma^+$, $6\ ^2\Pi$, $10\ ^2\Sigma^+$, $7\ ^2\Pi$, $11\ ^2\Sigma^+$, $8\ ^2\Pi$, $12\ ^2\Sigma^+$, $9\ ^2\Pi$, $13\ ^2\Sigma^+$, $14\ ^2\Sigma^+$, and $10\ ^2\Pi$ are taken into account. Thirty-eight nonadiabatic radial couplings and 40 rotational couplings are involved in the current calculations. Test calculations using a larger set of molecular states, as given in Table I, found the capture cross sections to the remaining states to be negligible for the considered energy range. Those states correlating to the $n=3$ and 4 manifolds have very-short-range interactions and will only contribute for energies greater than ~ 10 keV/u, while the states correlating to $6d$, $6f$, and $6g$ and the $n=7$ manifold have very-

TABLE I. Comparison of asymptotic separated-atom energies (in eV) between the *ALCHEMY* calculations and experiment for ClH^{7+} . The 38 molecular states are of symmetries $^2\Sigma^+$ and $^2\Pi$.

Asymptotic atomic state	Mol. state	This work	Expt. [19]
$\text{Cl}^{6+}(2p^63s\ ^2S)+\text{H}^+$	$1\ ^2\Sigma^+$	-99.7719	-100.6026
$\text{Cl}^{6+}(2p^63p\ ^2P^o)+\text{H}^+$	$2\ ^2\Sigma^+$	-84.6436	-85.1952
	$1\ ^2\Pi$	-84.6422	
$\text{Cl}^{6+}(2p^63d\ ^2D)+\text{H}^+$	$3\ ^2\Sigma^+$	-64.0412	-64.6201
	$2\ ^2\Pi$	-64.0408	
$\text{Cl}^{6+}(2p^64s\ ^2S)+\text{H}^+$	$4\ ^2\Sigma^+$	-42.7737	-43.0736
$\text{Cl}^{6+}(2p^64p\ ^2P^o)+\text{H}^+$	$5\ ^2\Sigma^+$	-37.2018	-37.4133
	$3\ ^2\Pi$	-37.1967	
$\text{Cl}^{6+}(2p^64d\ ^2D)+\text{H}^+$	$6\ ^2\Sigma^+$	-29.7875	-30.0350
	$4\ ^2\Pi$	-29.7859	
$\text{Cl}^{6+}(2p^64f\ ^2F^o)+\text{H}^+$	$7\ ^2\Sigma^+$	-28.1147	-28.1843
	$5\ ^2\Pi$	-28.1142	
$\text{Cl}^{6+}(2p^65s\ ^2S)+\text{H}^+$	$8\ ^2\Sigma^+$	-20.1624	-20.3009
$\text{Cl}^{6+}(2p^65p\ ^2P^o)+\text{H}^+$	$9\ ^2\Sigma^+$	-17.5044	-17.6088
	$6\ ^2\Pi$	-17.4910	
$\text{Cl}^{6+}(2p^65d\ ^2D)+\text{H}^+$	$10\ ^2\Sigma^+$	-13.9801	-14.1099
	$7\ ^2\Pi$	-13.9750	
$\text{Cl}^{6+}(2p^65f\ ^2F^o)+\text{H}^+$	$11\ ^2\Sigma^+$	-13.1355	-13.1436
	$8\ ^2\Pi$	-13.1328	
$\text{Cl}^{6+}(2p^65g\ ^2G)+\text{H}^+$	$12\ ^2\Sigma^+$	-13.0266	-13.0768
	$9\ ^2\Pi$	-13.0274	
$\text{Cl}^{6+}(2p^66s\ ^2S)+\text{H}^+$	$13\ ^2\Sigma^+$	-8.8827	-8.8915
$\text{Cl}^{6+}(2p^66p\ ^2P^o)+\text{H}^+$	$14\ ^2\Sigma^+$	-7.4038	-7.4582
	$10\ ^2\Pi$	-7.3766	
$\text{Cl}^{7+}(2p^6\ ^1S)+\text{H}$	$15\ ^2\Sigma^+$	0.0000	0.0000
$\text{Cl}^{6+}(2p^66d\ ^2D)+\text{H}^+$	$16\ ^2\Sigma^+$	-5.4825	-5.5278
	$11\ ^2\Pi$	-5.4688	
$\text{Cl}^{6+}(2p^66f\ ^2F^o)+\text{H}^+$	$17\ ^2\Sigma^+$	-5.0138	-4.9679
	$12\ ^2\Pi$	-5.0091	
$\text{Cl}^{6+}(2p^66g\ ^2G)+\text{H}^+$	$18\ ^2\Sigma^+$	-4.8323	-4.9278
	$13\ ^2\Pi$	-4.8338	
$\text{Cl}^{6+}(2p^67s\ ^2S)+\text{H}^+$	$19\ ^2\Sigma^+$	-2.4611	
$\text{Cl}^{6+}(2p^67p\ ^2P^o)+\text{H}^+$	$20\ ^2\Sigma^+$	-1.5711	
	$14\ ^2\Pi$	-1.5265	
$\text{Cl}^{6+}(2p^67d\ ^2D)+\text{H}^+$	$21\ ^2\Sigma^+$	-0.4246	
	$15\ ^2\Pi$	-0.3979	
$\text{Cl}^{6+}(2p^67f\ ^2F^o)+\text{H}^+$	$22\ ^2\Sigma^+$	-0.0896	
	$16\ ^2\Pi$	-0.0849	

long-range avoided-crossings with the entrance channel and can be considered completely diabatic. In Figs. 2 and 3, nine representative nonadiabatic radial couplings and eight representative rotational couplings are plotted as a function of R . The potentials have been transformed from the adiabatic representation to the diabatic representation. The diagonal diabatic potential energies (dashed curves) are illustrated in Fig. 1, and representative off-diagonal matrix elements are given in Fig. 4. We will discuss how the diabatic potentials are obtained in the next section.

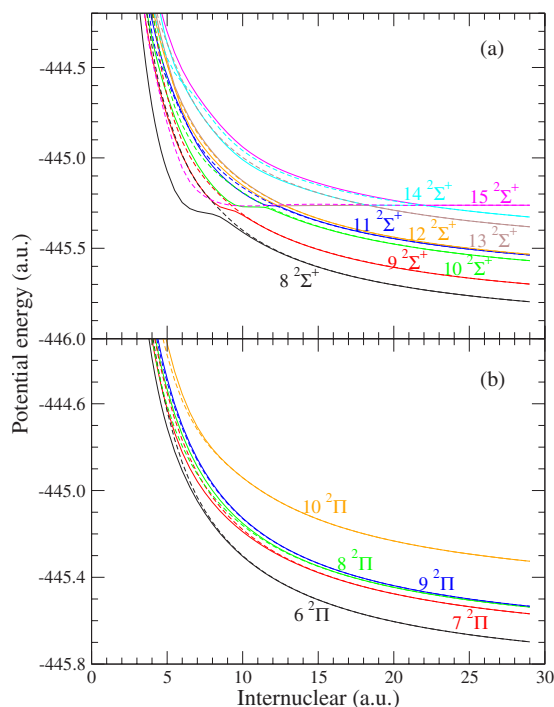


FIG. 1. (Color online) Adiabatic (solid line) and diagonal diabatic (dashed line) potential energies of the CIH^{7+} system as a function of internuclear distance R .

Beyond $R=29.0$ a.u., the potentials for the entrance channels are described by the charge-induced-dipole interactions

$$V_L(R) = -\frac{\alpha_d}{2R^4} + E_\infty, \quad (2)$$

where α_d is the dipole polarizability of neutral H and E_∞ is the separated-atom energy. All quantities in Eq. (2) are in atomic units (a.u.). For all exit channels, the long-range potentials ($R > 29.0$ a.u.) are Coulombic. E_∞ is determined using the α_d parameter and the *ab initio* potentials.

III. SCATTERING THEORY

A QMOCC approach to describe electron capture in ion-atom collisions has been formulated by Kimura and Lane [8] and Zygelman *et al.* [9]. Here only a brief summary of its main theoretical aspects and formulas is given.

The QMOCC approach involves solving a coupled set of second-order differential equations. Its solutions are the expansion coefficients, or scattering amplitudes, of the total system wave function expanded over a truncated set of adiabatic molecular eigenfunctions. In the adiabatic representation, transitions from a molecular state to another molecular state are driven by the vector potential $A(\mathbf{R})$, where \mathbf{R} is the coordinate of the relative nuclear motion. However, it is numerically more convenient to perform the scattering calculations in a diabatic representation which can be obtained with a unitary transformation. By making the unitary transformation, the set of the coupled equations in the diabatic representation is given by

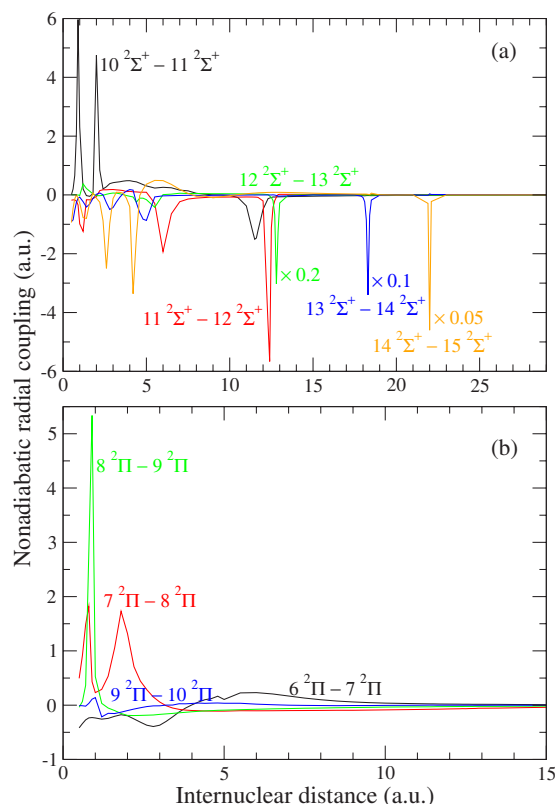


FIG. 2. (Color online) Representative (a) ${}^2\Sigma^+$ and (b) ${}^2\Pi$ nonadiabatic radial couplings for the CIH^{7+} system as a function of internuclear distance R . Note that the peak values of some couplings in (a) have been multiplied by a constant.

$$-\frac{1}{2\mu}\nabla^2 G(\mathbf{R}) + U(R)G(\mathbf{R}) = EG(\mathbf{R}), \quad (3)$$

where μ is the nuclear reduced mass of the ion-atom pair, E is the relative collision energy in the center-of-mass frame, $G(\mathbf{R})$ is the scattering amplitude describing relative motion of the nuclei, and $U(R)$ with $R=|\mathbf{R}|$ is the diabatic potential matrix, whose off-diagonal elements are responsible for driving charge transfer reactions in the diabatic representation, defined by

$$U(R) = W(R)[V(R) - P(R)]W^{-1}(R), \quad (4)$$

where $V(R)$ is a diagonal matrix with elements consisting of adiabatic eigenvalues for each channel state, $W(R)$ is a unitary matrix that obeys the equation

$$\frac{dW(R)}{dR} + iW(R)A^{rad}(R) = 0, \quad (5)$$

and $P(R)$ is a coupling matrix whose elements are given by [20,21]

$$P_{\alpha\beta} = \mp \frac{1}{\mu R^2} [(J \mp \Lambda_\alpha)(J \pm \Lambda_\alpha + 1)]^{1/2} A_{\alpha\beta}^{rot} \delta(\Lambda_\alpha, \Lambda_\beta \mp 1), \quad (6)$$

where J is the total angular momentum, Λ is the component of electronic angular momenta along the internuclear axis,

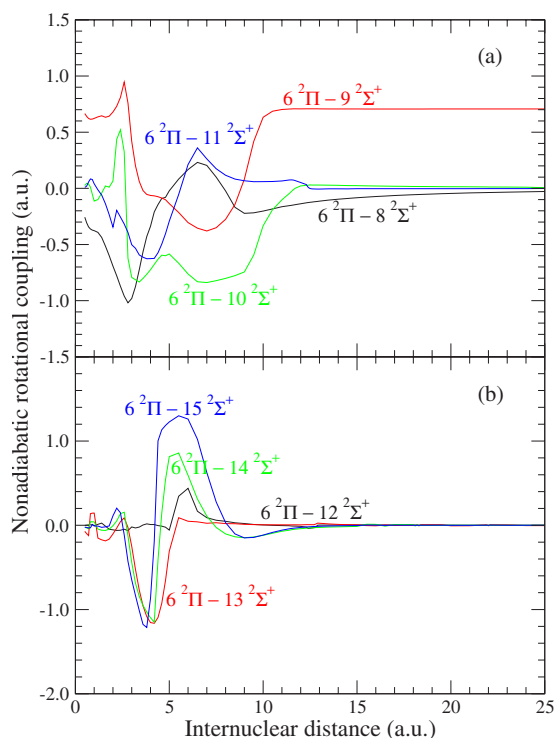


FIG. 3. (Color online) Representative nonadiabatic rotational couplings between the ${}^2\Pi$ and ${}^2\Sigma^+$ states of the CIH^{7+} system as a function of internuclear distance R .

and $A^{rad}(R)$ and $A^{rot}(R)$ are, respectively, the radial and rotational components of the vector potential $[A(\mathbf{R})]_{\alpha\beta} = i\langle\psi_\alpha|\nabla_{\mathbf{R}} + \sum_k f(\mathbf{r}_k; \mathbf{R})\nabla_{\mathbf{r}_k}|\psi_\beta\rangle$ with ψ_α and ψ_β being the adiabatic electronic eigenfunctions. The second term in the vector potential is due to the introduction of an electron translation factor (see, for example, Refs. [17,22].) where \mathbf{r}_k is the coordinate for electron k and $f(\mathbf{r}_k; \mathbf{R})$ is a so-called switching function defined as in Watanabe *et al.* [17]. The introduction of the translation factor ensures that all asymptotic radial and rotational couplings go to zero even for dipole-connected asymptotic atomic states as seen in Figs. 2 and 3.

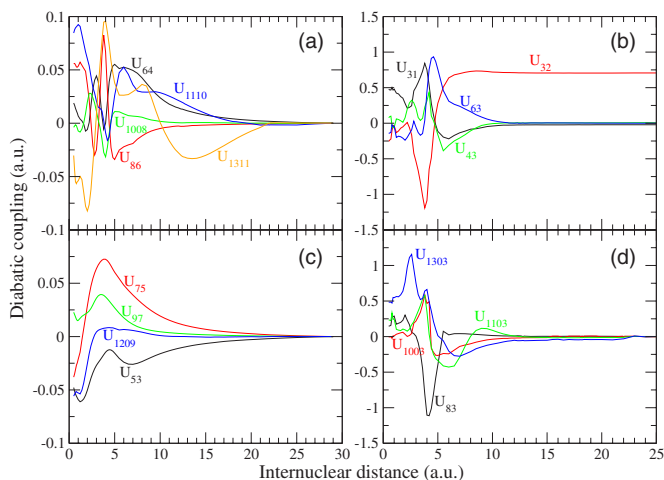


FIG. 4. (Color online) Representative off-diagonal diabatic potentials of the CIH^{7+} system as a function of internuclear distance R .

By introducing a partial-wave decomposition for $G(\mathbf{R})$, Eq. (3) can be further simplified. The resulting set of radial coupled equations may be solved with the log-derivative method of Johnson [23]. From the numerical results of the log-derivative and the asymptotic expressions of the radial functions, the K matrix may be extracted and thus the scattering matrix S is obtained:

$$S_J = [I + iK_J]^{-1}[I - iK_J]. \quad (7)$$

Finally the charge-transfer cross section from channel α to channel β is expressed in terms of the scattering matrix elements

$$\sigma_{\alpha\rightarrow\beta} = \frac{\pi g_\alpha}{k_\alpha^2} \sum_J (2J+1) |(S_J)_{\alpha\beta}|^2, \quad (8)$$

where k_α denotes the wave number for center-of-mass motion of the initial ion-atom channel and g_α is an approach probability factor of the initial channel α .

IV. RESULTS AND DISCUSSION

A 13-channel close-coupling calculation was performed using the molecular electronic structure and coupling data presented in Sec. II. Eight states of the 13 channels are of symmetry ${}^2\Sigma^+$ and five states of symmetry ${}^2\Pi$. Only electron capture into 6ℓ with $\ell=s$ and p and all 5ℓ orbitals of $\text{Cl}^{6+}(2p^6n\ell)$ are included. The contributions from the individual partial waves are summed as in Eq. (8) until a convergence of the cross sections is achieved. Since the speed of convergence depends on the relative collision energy, the computations are satisfactorily fast for low energy, but become prohibitively lengthy above a few 100 eV/u because of the increase in the number of partial waves.

State-to-state cross sections are illustrated in Fig. 5, (a) and (b) corresponding, respectively, to capture into the ${}^2\Sigma^+$ states via radial coupling and into the ${}^2\Pi$ states through rotational coupling from the entrance channel $15 {}^2\Sigma^+$. Figure 5 shows that capture into the $10 {}^2\Sigma^+$, $11 {}^2\Sigma^+$, $12 {}^2\Sigma^+$, $13 {}^2\Sigma^+$, and $14 {}^2\Sigma^+$ states is dominant below 0.1 eV/u. This is easily interpreted from Fig. 1(a) where the avoided-crossings of the adiabatic potentials of these states and the entrance channel occurs in the large- R (>10 a.u.) range. The avoided crossings correspond to sharp peaks of the radial couplings in Fig. 2(a), such as at $R=18.3$ and 22.0 a.u. This illustrates that there exist strong couplings among these channels, which result in the dominant charge-transfer transitions. It should be emphasized that we used Lorentzian profiles to replace the three largest radial couplings at $R=12.8$, 18.3 , and 22.0 a.u. to prevent unphysical oscillations in the interpolation of the couplings in the sharp avoided-crossing regions. Above about 0.1 eV/u, charge transfer due to rotational coupling such as $15 {}^2\Sigma^+ \rightarrow 6 {}^2\Pi$, $7 {}^2\Pi$, and $10 {}^2\Pi$ begins to become important and is comparable to that due to radial coupling at 10.0 eV/u. This is because the possibility for the system to penetrate the inner region with small and intermediate R becomes larger with increasing collision energy, while stronger couplings between the molecular states occur for $R < 10.0a_0$ as seen in Fig. 3.

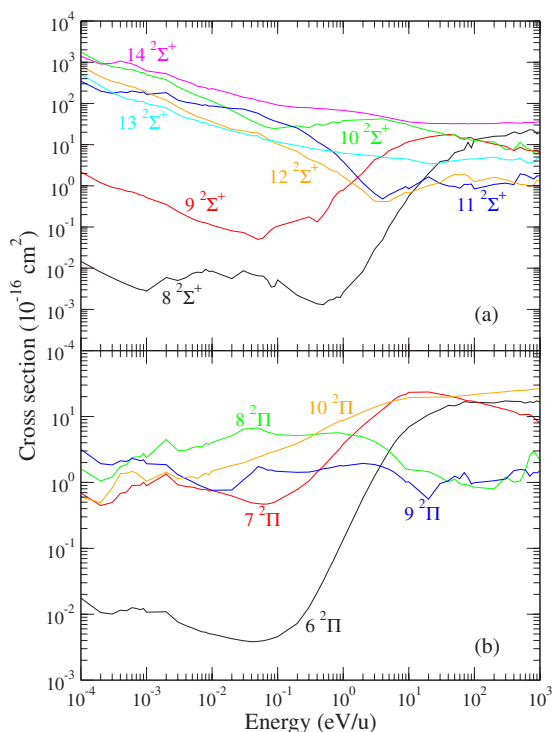


FIG. 5. (Color online) State-to-state QMOCC electron-capture cross sections for the CIH^{7+} system as a function of relative collision energy E . (a) and (b) corresponding to transitions from the entrance channels to all seven ${}^2\Sigma^+$ states and five ${}^2\Pi$ states, respectively.

To gain insight into the dominant physical processes, Thompson *et al.* [13] performed a multichannel Landau-Zener analysis of the diabatic potentials for CID^{7+} and suggested that capture into the $4d$ and $4f$ states dominated charge transfer in the 20–1000 eV/u energy range and that the $5s$ state begins to contribute to the cross sections below 20 eV/u. Although such a conclusion, which depends on the form of the adopted empirical couplings [13], was found to agree qualitatively with a fully quantal molecular-orbital close-coupling hidden-crossing (FQ-MOCC-HC) theoretical analysis for the ND^{7+} system, it is different from our computational results for the CIH^{7+} system. The current QMOCC and potential calculations show that the contributions from electron capture into the 3ℓ , 4ℓ , $6d$, $6f$, $6g$, and 7ℓ orbitals are negligible. In order to compare the contribution from capture into the 5ℓ , $6s$, and $6p$ orbitals involved in the current calculation, the state-selective cross sections are plotted in Fig. 6. It is seen that the $5d$, $5f$, $5g$, and $6p$ dominate the charge-transfer processes over the entire energy range considered and the $5s$ and $5p$ begin to become important only above a few eV/u. The $6s$ is seen to be only important at energies less than 10^{-3} eV.

An empirical ℓ -distribution function for charge-transfer reactions was proposed by Abramov *et al.* [24] and widely utilized in plasma modeling [3]. However, few theoretical examinations of such a distribution have been made. Here we check the validity of the ℓ -distribution function by comparing with our *ab initio* QMOCC results. The function is written in the form

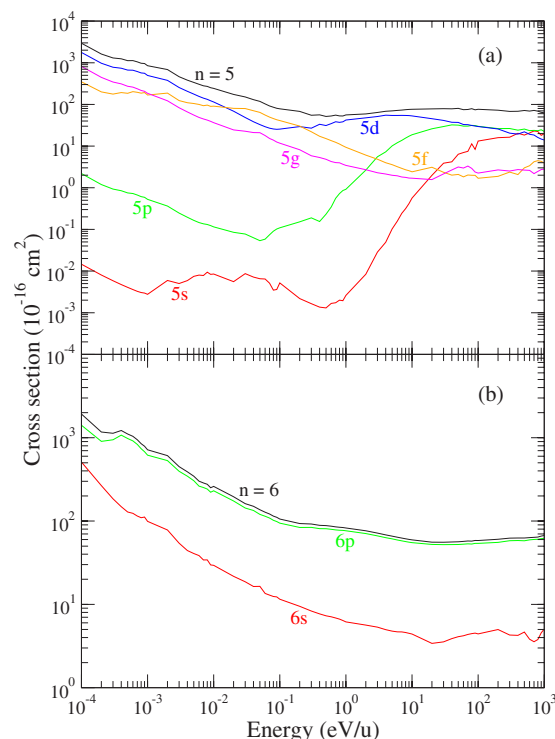


FIG. 6. (Color online) State-selective electron-capture cross sections as a function of relative collision energy E . (a) and (b) correspond to capture into $\text{Cl}^{6+}(2p^6 5\ell)$ and $\text{Cl}^{6+}(2p^6 6\ell)$.

$$W_{n\ell} = (2\ell + 1) \frac{[(n-1)!]^2}{(n+\ell)! (n-1-\ell)!}. \quad (9)$$

This equation is explicitly independent of collision energy, but thought to be suitable for the low-energy range below 1 keV/u. Furthermore, it is strictly relevant to single-electron systems, but has been widely, and usually incorrectly, adopted for multielectron ions [3]. In Fig. 7, the distribution function of Abramov *et al.*, $W_{n\ell}$, for $n=5$ is plotted along

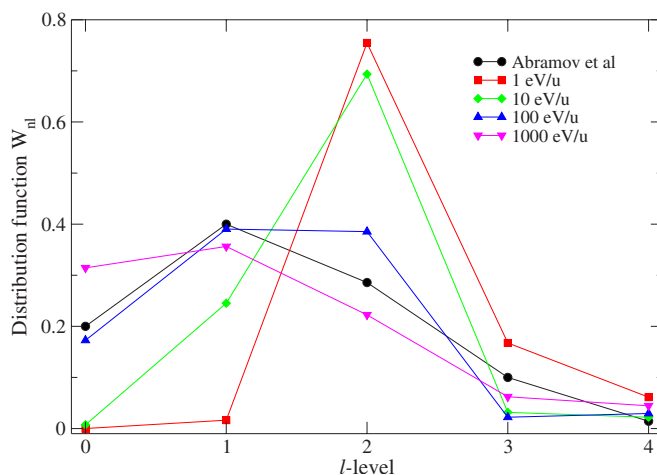


FIG. 7. (Color online) Comparison of ℓ distributions for the charge-transfer reaction $\text{Cl}^{7+} + \text{H} \rightarrow \text{Cl}^{6+}(2p^6 n\ell, n=5) + \text{H}^+$ between the calculation from Eq. (9) and the QMOCC results at 1, 10, 100, and 1000 eV/u.

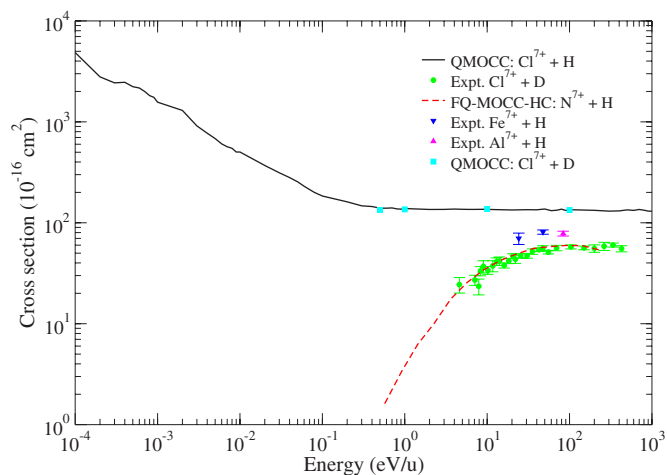


FIG. 8. (Color online) Total electron-capture cross sections as a function of relative collision energy E . A comparison is shown with the measurements for the $\text{Cl}^{7+}+\text{D}$ [13], $\text{Fe}^{7+}+\text{H}$ [14], and $\text{Al}^{7+}+\text{H}$ [15] systems and with the fully quantal molecular-orbital close-coupling hidden-crossing calculation (FQ-MOCC-HC) for the $\text{N}^{7+}+\text{D}$ system [13]. $\text{Cl}^{7+}+\text{D}$ QMOCC results are also given.

with our *ab initio* QMOCC results at $E=1, 10, 100$, and 1000 eV/u. The comparison shows a strong energy dependence for the ℓ distribution with the function of Abramov *et al.* being reasonably accurate for $100\text{--}1000$ eV/u, but failing for smaller collision energies. This suggests that care must be exercised when using empirical distribution functions particularly when the energy range of applicability is not clearly defined. Furthermore, it is expected that as the collision energy exceeds 10 keV/u, the ℓ levels should be populated by a statistical distribution given by

$$W_{nl}^{\text{st}} = (2\ell + 1)/n^2. \quad (10)$$

The QMOCC results displayed in Fig. 7, suggest that even up to as high as 1 keV/u, the ℓ distribution for Cl^{7+}/H is far from statistical.

The total QMOCC charge transfer cross section due to collisions of Cl^{7+} with H are compared with the measured cross sections for the $\text{Cl}^{7+}+\text{D}$ system and theoretical cross sections for the $\text{N}^{7+}+\text{D}$ system in Fig. 8 [13]. An obvious discrepancy is seen between the current QMOCC calculations and the measurement. In the low-energy range, the discrepancy may be attributed to the kinematic isotope effect, which was found to be very significant for charge transfer between N^{4+} and $\text{H}(\text{D})$ [25]. However, it has been shown that in a higher-energy range, such as for collision energies greater than ~ 50 eV/u, the H and D cross sections become quantitatively indistinguishable. The current QMOCC cross sections are larger than the measured cross sections approximately by a factor of 2 above ~ 50 eV/u. To ensure that the difference with experiment is not due to an isotope effect, we performed additional calculations using the $\text{Cl}^{7+}+\text{D}$ reduced mass in Eq. (3) for energies between 0.5 and 100 eV/u. As shown in Fig. 8, the results are practically identical to the $\text{Cl}^{7+}+\text{H}$ calculation. Similarly, the FQ-MOCC-HC calculations in Ref. [13] revealed no significant isotope effect for $\text{N}^{7+}+\text{H}$ or D in the considered energy range.

Although the molecular-orbital close-coupling hidden-crossing calculation for $\text{N}^{7+}+\text{D}$ seems to support the experimental data for $\text{Cl}^{7+}+\text{D}$, such support may be weak because it assumes that effects of the closed $[\text{Ne}]$ core are negligible without theoretical justification. In contrast to such an assumption, a comparison between the FQ-MOCC-HC calculation and the current QMOCC results suggests that the electronic structure of the closed $[\text{Ne}]$ shell has a significant effect on the electron capture cross sections. Such a result is expected upon consideration of the potential energies given in Fig. 1, where interaction with the $[\text{Ne}]$ core removes the degeneracy in the Cl^{6+} $n=5$ and 6 manifolds, unlike in the hydrogenlike N^{6+} case. The avoided crossing for the N^{6+} $n=5$ state occurs near 11.5 a.u. [13], while for the Cl^{6+} $n=5$ manifold, the $5s\text{--}5g$ avoided crossings for each individual ℓ channel occur at $\sim 8, 9.2, 11.5, 12.4$, and 12.8 a.u., respectively. For $n=6$, the N^{6+} avoided crossing occurs at 33 a.u., while the $6s\text{--}6g$ avoided crossings for Cl^{6+} are located at $18.3, 22.0, 29.5, 32.8$, and 33.1 a.u., respectively. The FQ-MOCC-HC calculations revealed that the low-energy cross section was dominated by the single capture channel, $n=5$, for $\text{N}^{7+}+\text{D}$, while our QMOCC calculation in Fig. 6 shows that up to seven capture channels contribute to the $\text{Cl}^{7+}+\text{H}$ cross section between 1 and 1000 eV/u. Clearly, the differences between the two theoretical results is consistent with the differences in molecular structure and the larger number of capture channels in the former, as expected. We note that there is a lack of other data for $\text{N}^{7+}+\text{H}$ below ~ 60 eV/u or for other $7+$ systems. Prior information on $\text{Cl}^{7+}+\text{H}$ is limited to the measurement in Ref. [13].

From Fig. 8, a hint of this core interaction is evident in the experimental results for $\text{Fe}^{7+}(4s)+\text{H} \rightarrow \text{Fe}^{6+}(4snl)+\text{H}^+$ [14] and $\text{Al}^{7+}(2p^2)+\text{H} \rightarrow \text{Al}^{6+}(2p^2nl)+\text{H}^+$ [15], which have larger total cross sections than the measured Cl^{7+}/D or calculated N^{7+}/D cases. Furthermore, it was pointed out in Thompson *et al.* [13] that merged-beam measurements for B^{4+} , C^{4+} , N^{4+} , and Si^{4+} resulted in cross sections that varied by as much as a factor of 10 at 1 eV/u. This core effect was predicted by Gargaud and McCarroll [26] who performed QMOCC calculations for C^{4+} , O^{4+} , and Si^{4+} with H. They commented that “charge transfer cross sections are critically dependent on the nature of the ionic core at energies less than a few 100 eV/u,” consistent with the results found in the current work.

It is beyond the scope of this work to perform a detailed analysis of the experimental conditions in Ref. [13]. However, a similar discrepancy between low-energy merged-beam measurements and QMOCC calculations was found for $\text{O}^{5+}+\text{H}$. This was explained by Andersson *et al.* [27], who showed from the study of differential cross sections that the experimental angular acceptance was insufficient for a collection of all scattered ions. Such an explanation may be possible for the Cl^{7+}/D measurements.

Rate coefficients are evaluated by averaging the QMOCC cross sections in Figs. 6(a) and 6(b) over a Maxwellian velocity distribution. The results are tabulated in Table II. The temperature ranges from 10 to 2.0×10^5 K. For convenience, the rate coefficients are fitted to the form

TABLE II. Rate coefficients for electron capture into the $\text{Cl}^{6+}(2p^6n\ell \ ^2S, \ ^2P^o, \ ^2D, \ ^2F^o, \ ^2G)+\text{H}^+$ channels due to $\text{Cl}^{7+}(2p^6 \ ^1S)+\text{H}$ collisions. T is in K and the rate coefficients are in cm^3/s . "Total" represents the rate coefficients summed over all exit channels.

T	$5s \ ^2S$	$5p \ ^2P^o$	$5d \ ^2D$	$5f \ ^2F^o$	$5g \ ^2G$	$6s \ ^2S$	$6p \ ^2P^o$	Total
10	2.18(-14) ^a	2.20(-12)	2.08(-09)	7.65(-10)	7.73(-10)	4.32(-10)	2.79(-09)	6.85(-09)
20	3.80(-14)	2.04(-12)	2.02(-09)	9.03(-10)	7.02(-10)	4.28(-10)	2.94(-09)	6.99(-09)
30	5.24(-14)	1.92(-12)	1.93(-09)	9.78(-10)	6.52(-10)	4.23(-10)	2.99(-09)	6.98(-09)
40	6.38(-14)	1.85(-12)	1.86(-09)	1.04(-09)	6.18(-10)	4.21(-10)	3.04(-09)	6.98(-09)
50	7.30(-14)	1.80(-12)	1.79(-09)	1.10(-09)	5.95(-10)	4.21(-10)	3.09(-09)	7.00(-09)
60	8.07(-14)	1.77(-12)	1.74(-09)	1.15(-09)	5.78(-10)	4.21(-10)	3.13(-09)	7.02(-09)
70	8.75(-14)	1.75(-12)	1.70(-09)	1.20(-09)	5.66(-10)	4.22(-10)	3.17(-09)	7.06(-09)
80	9.38(-14)	1.73(-12)	1.66(-09)	1.25(-09)	5.57(-10)	4.23(-10)	3.21(-09)	7.09(-09)
90	9.95(-14)	1.73(-12)	1.62(-09)	1.29(-09)	5.51(-10)	4.25(-10)	3.24(-09)	7.12(-09)
100	1.05(-13)	1.72(-12)	1.59(-09)	1.33(-09)	5.47(-10)	4.26(-10)	3.26(-09)	7.15(-09)
200	1.42(-13)	1.85(-12)	1.37(-09)	1.58(-09)	5.45(-10)	4.42(-10)	3.46(-09)	7.39(-09)
300	1.62(-13)	2.19(-12)	1.28(-09)	1.68(-09)	5.50(-10)	4.55(-10)	3.60(-09)	7.57(-09)
400	1.75(-13)	2.67(-12)	1.25(-09)	1.74(-09)	5.51(-10)	4.66(-10)	3.74(-09)	7.74(-09)
500	1.83(-13)	3.21(-12)	1.25(-09)	1.77(-09)	5.49(-10)	4.76(-10)	3.86(-09)	7.91(-09)
600	1.87(-13)	3.78(-12)	1.28(-09)	1.78(-09)	5.46(-10)	4.86(-10)	3.99(-09)	8.09(-09)
700	1.88(-13)	4.36(-12)	1.32(-09)	1.79(-09)	5.42(-10)	4.96(-10)	4.12(-09)	8.27(-09)
800	1.88(-13)	4.95(-12)	1.36(-09)	1.80(-09)	5.38(-10)	5.05(-10)	4.25(-09)	8.46(-09)
900	1.87(-13)	5.56(-12)	1.41(-09)	1.80(-09)	5.34(-10)	5.14(-10)	4.38(-09)	8.64(-09)
1000	1.86(-13)	6.19(-12)	1.46(-09)	1.79(-09)	5.30(-10)	5.23(-10)	4.51(-09)	8.83(-09)
2000	1.77(-13)	1.57(-11)	2.08(-09)	1.72(-09)	5.03(-10)	5.95(-10)	5.70(-09)	1.06(-08)
3000	2.03(-13)	3.29(-11)	2.73(-09)	1.64(-09)	4.92(-10)	6.50(-10)	6.67(-09)	1.22(-08)
4000	2.70(-13)	5.80(-11)	3.37(-09)	1.57(-09)	4.88(-10)	6.97(-10)	7.49(-09)	1.37(-08)
5000	3.89(-13)	9.17(-11)	3.98(-09)	1.52(-09)	4.88(-10)	7.38(-10)	8.19(-09)	1.50(-08)
6000	5.71(-13)	1.34(-10)	4.56(-09)	1.48(-09)	4.90(-10)	7.76(-10)	8.82(-09)	1.62(-08)
7000	8.29(-13)	1.84(-10)	5.10(-09)	1.44(-09)	4.93(-10)	8.11(-10)	9.37(-09)	1.74(-08)
8000	1.18(-12)	2.42(-10)	5.61(-09)	1.41(-09)	4.96(-10)	8.43(-10)	9.88(-09)	1.85(-08)
9000	1.63(-12)	3.06(-10)	6.10(-09)	1.39(-09)	4.99(-10)	8.74(-10)	1.03(-08)	1.95(-08)
10000	2.21(-12)	3.77(-10)	6.56(-09)	1.37(-09)	5.03(-10)	9.02(-10)	1.08(-08)	2.05(-08)
20000	1.71(-11)	1.30(-09)	1.03(-08)	1.25(-09)	5.43(-10)	1.13(-09)	1.40(-08)	2.85(-08)
30000	5.32(-11)	2.42(-09)	1.30(-08)	1.20(-09)	5.81(-10)	1.29(-09)	1.62(-08)	3.47(-08)
40000	1.12(-10)	3.59(-09)	1.51(-08)	1.20(-09)	6.16(-10)	1.41(-09)	1.79(-08)	4.00(-08)
50000	1.91(-10)	4.74(-09)	1.68(-08)	1.21(-09)	6.53(-10)	1.51(-09)	1.95(-08)	4.46(-08)
60000	2.89(-10)	5.87(-09)	1.82(-08)	1.24(-09)	6.93(-10)	1.60(-09)	2.09(-08)	4.88(-08)
70000	4.01(-10)	6.95(-09)	1.94(-08)	1.28(-09)	7.37(-10)	1.68(-09)	2.22(-08)	5.26(-08)
80000	5.26(-10)	7.99(-09)	2.04(-08)	1.31(-09)	7.85(-10)	1.75(-09)	2.34(-08)	5.62(-08)
90000	6.61(-10)	8.98(-09)	2.13(-08)	1.35(-09)	8.37(-10)	1.83(-09)	2.46(-08)	5.96(-08)
100000	8.06(-10)	9.94(-09)	2.21(-08)	1.38(-09)	8.92(-10)	1.90(-09)	2.57(-08)	6.27(-08)
200000	2.71(-09)	1.75(-08)	2.75(-08)	1.63(-09)	1.48(-09)	2.60(-09)	3.52(-08)	8.86(-08)

^a $A(-B)=A \times 10^{-B}$.

$$\alpha(T) = \sum_i a_i \left(\frac{T}{10\ 000} \right)^{b_i} \exp\left(-\frac{T}{c_i}\right), \quad (11)$$

where α is the rate coefficient in cm^3/s and T is temperature in K. The fitting parameters a_i (cm^3/s), b_i , and c_i (K) are given in Table III. In the temperature range considered, the fits do not deviate from the computed rate coefficients by more than 24.2%, 16.2%, 16.6%, 9.7%, 7.0%, 0.7%, 5.0%, and 3.0% for electron capture into the $5s \ ^2S$, $5p \ ^2P^o$, $5d \ ^2D$,

$5f \ ^2F^o$, $5d \ ^2G$, $6s \ ^2S$, and $6p \ ^2P^o$ states of $\text{Cl}^{6+}(2p^6n\ell)$, and the summed exit channels, respectively.

V. SUMMARY

Charge transfer has been investigated for collisions of Cl^{7+} and H based on the quantal molecular-orbital close-coupling approach. The configuration-interaction method was used to evaluate the molecular electronic structure and

TABLE III. Fitting parameters of rate coefficients for capture into $\text{Cl}^{6+}(2p^6n\ell\ ^2S, ^2P^o, ^2D, ^2F^o, ^2G)+\text{H}^+$ channels and the summed exit channels (Total) due to $\text{Cl}^{7+}(2p^6\ ^1S)+\text{H}$ collisions. T is in K; and a_i and c_i are in units of cm^3/s and K, respectively.

Param.	$5s\ ^2S$	$5p\ ^2P^o$	$5d\ ^2D$	$5f\ ^2F^o$	$5g\ ^2G$	$6s\ ^2S$	$6p\ ^2P^o$	Total
a_1	2.5997(-12) ^a	3.9231(-10)	6.5199(-09)	1.0037(-09)	3.4663(-10)	6.3211(-10)	8.4735(-09)	1.4656(-08)
b_1	2.9165(+00)	1.9538(+00)	9.6442(-01)	1.3737(-01)	7.8431(-02)	4.7284(-01)	5.9359(-01)	7.0547(-01)
c_1	1.0987(+05)	7.7302(+04)	8.3387(+04)	-9.3204(+06)	-2.0014(+05)	2.8849(+05)	1.6200(+05)	2.1728(+05)
a_2	1.4413(-12)	1.5820(-12)	4.7009(-10)	2.4833(-09)	1.3895(-10)	2.6759(-10)	2.3249(-09)	5.6402(-09)
b_2	5.7480(-01)	-2.7907(-02)	-2.3686(-01)	2.5637(-01)	-1.9133(-01)	-6.1187(-02)	-2.6475(-02)	-3.0024(-02)
cc_2	1.5419(+03)	-2.3482(+04)	-4.6553(+04)	4.4044(+03)	-1.3881(+05)	-1.1338(+05)	-8.8121(+04)	-9.7076(+04)

^a $A(-B)=A \times 10^{-B}$.

coupling matrix elements between the adiabatic molecular states for the ClH^{7+} system. Cross sections are presented for electron capture into the exit channels $\text{Cl}^{6+}(2p^6n\ell)+\text{H}^+$ for collisions of $\text{Cl}^{7+}(2p^6\ ^1S)$ with H at collision energies between 0.1 meV/u and 1 keV/u. Rate coefficients are given for temperatures between 10 K and 2.0×10^5 K. The current QMOCC investigation shows that electron capture into $5d$, $5f$, $5g$, and $6p$ states dominates the cross section for collision energies less than 1 eV/u, while above 100 eV/u the $5s$, $5p$, $5d$, and $6p$ are the primary capture channels. Comparison with the experimental data for collisions of $\text{Cl}^{7+}(\ ^1S)$ and D reveal a large discrepancy, even for energies greater than ~ 50 eV/u where kinematic isotope effects are believed to be negligible [25]. Furthermore, we also compared the current QMOCC results with the fully quantal molecular-orbital hidden-crossing cross sections for the $\text{N}^{7+}+\text{D}$ system as well

as with the measurements for the same charged $\text{Fe}^{7+}+\text{H}$ and $\text{Al}^{7+}+\text{H}$ systems. This accumulated evidence suggests that the electronic structure of the core has a non-negligible effect on the charge-transfer process. Further experimental investigations of collisions of Cl^{7+} with H (D) and of other multi-electron ions are needed.

ACKNOWLEDGMENTS

L.B.Z. and P.C.S. acknowledge support from NASA Grant No. NNG05GD98G and NSF Grant No. INT-0300708 and M.K. from the Ministry of Education, Science, Sport, Culture and Technology, Japan Society for Promotion of Science (JSPS) for the U.S.-JP Collaborative Research Program and Collaborative Research Grant by the National Institute for Fusion Science.

- [1] R. K. Janev, *Review of Fundamental Processes and Applications of Atoms and Ions* (World Scientific, Singapore, 1993).
- [2] G. J. Ferland, *Annu. Rev. Astron. Astrophys.* **41**, 517 (2003).
- [3] V. A. Krasnopolsky, J. B. Greenwood, and P. C. Stancil, *Space Sci. Rev.* **113**, 271 (2004), and references therein.
- [4] C. M. Lisse, D. J. Christian, K. Dennerl, K. J. Meech, R. Petre, H. A. Weaver, and S. J. Wolk, *Science* **292**, 1343 (2001).
- [5] F. P. Keenan, C. A. Ramsbottom, K. L. Bell, K. A. Berrington, A. Hibbert, W. A. Feibelman, and W. P. Blair, *Astrophys. J.* **438**, 500 (1995).
- [6] A. D. Silber, S. F. Anderson, B. Margon, and R. A. Downers, *Astrophys. J.* **462**, 428 (1996).
- [7] J. Caillat, A. Dubois, I. Sundvor, and J.-P. Hansen, *Phys. Rev. A* **70**, 032715 (2004).
- [8] M. Kimura and N. F. Lane, *Adv. At., Mol., Opt. Phys.* **26**, 79 (1990).
- [9] B. Zygelman, D. L. Cooper, M. J. Ford, A. Dalgarno, J. Gerratt, and M. Raimondi, *Phys. Rev. A* **46**, 3846 (1992).
- [10] W. Fritsch, *Phys. Rev. A* **35**, 2342 (1987); W. Fritsch and C. D. Lin, *Phys. Rep.* **202**, 1 (1991).
- [11] R. Abrines and I. C. Percival, *Proc. Phys. Soc. London* **88**, 861 (1966); R. E. Olson and A. Salop, *Phys. Rev. A* **16**, 531 (1977).
- [12] Dž Belkić, R. Gayet, and A. Salin, *Phys. Rep.* **56**, 279 (1979).
- [13] J. S. Thompson, A. M. Covington, P. S. Krstić, Marc Pieksma, J. L. Shinnpaugh, P. C. Stancil, and C.C. Havener, *Phys. Rev. A* **63**, 012717 (2000).
- [14] R. A. Phaneuf, *Phys. Rev. A* **28**, 1310 (1983).
- [15] R. A. Phaneuf, M. Kimura, H. Sato, and R. E. Olson, *Phys. Rev. A* **31**, 2914 (1985).
- [16] A. D. McLean, M. Yoshimine, B. H. Lengsfeld, P. S. Bagus, and B. Liu, *ALCHEMY II* (IBM, 1981).
- [17] A. Watanabe, R. Suzuki, H. Sato, and M. Kimura, *Nat. Sci. Rep. Ochanomizu Univ.* **49**, 2 (1998).
- [18] E. Clementi and C. Roetti, *At. Data Nucl. Data Tables* **14**, 177 (1974).
- [19] N. I. S. T. Atomic Spectra Database, <http://physics.nist.gov/asd>.
- [20] B. H. Bransden and M. R. C. McDowell, *Charge Exchange and the Theory of Ion-Atom Collisions* (Clarendon Press, Oxford, 1992).
- [21] A. R. Turner, D. L. Cooper, J. G. Wang, and P. C. Stancil, *Phys. Rev. A* **68**, 012704 (2003).
- [22] N. Shimakura and M. Kimura, *Phys. Rev. A* **44**, 1659 (1991).
- [23] B. R. Johnson, *J. Comput. Phys.* **13**, 445 (1973).
- [24] V. A. Abramov, F. F. Baryshnikov, and V. S. Lisitsa, *JETP Lett.* **27**, 464 (1978).
- [25] P. C. Stancil and B. Zygelman, *Phys. Rev. Lett.* **75**, 1495 (1995).
- [26] M. Gargaud and R. McCarroll, *J. Phys. B* **21**, 513 (1988).
- [27] L. R. Andersson, M. Gargaud, and R. McCarroll, *J. Phys. B* **24**, 2073 (1991).